ORGANIC CHEMISTRY

FRONTIERS

Accepted Manuscript

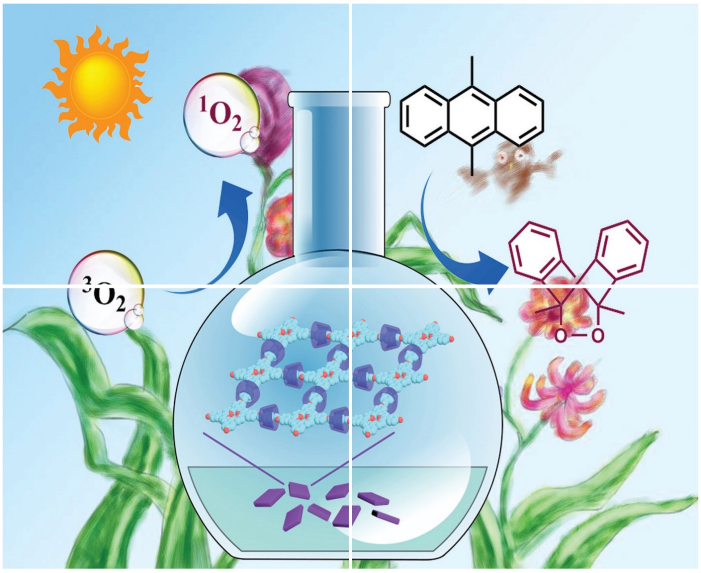

This article can be cited before page numbers have been issued, to do this please use: S. Kim, B. H. Jhun, Y. Lee, G. Lee, S. Woo, J. Bae, S. Lee, S. Kim, Y. You and E. J. Cho, *Org. Chem. Front.*, 2025, DOI: 10.1039/D5QO00774G.

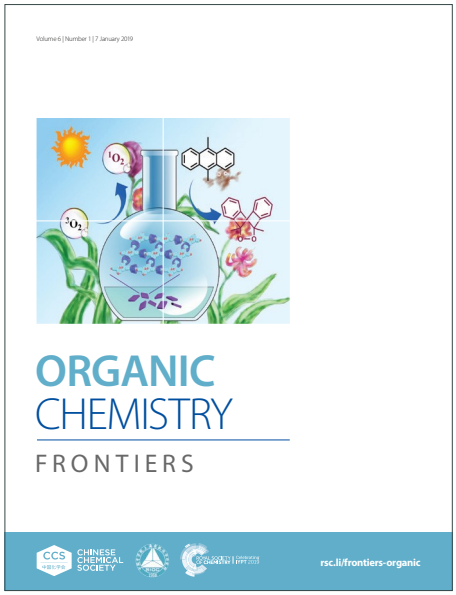

View Article Online
DOI: 10.1039/D5QO00774G

ARTICLE

Beyond Energy Transfer: Ground-State Association-Driven [2+2] Cycloadditions with Indole-Fused Organophotocatalysts

Received 00th January 20xx,
Accepted 00th January 20xx

DOI: 10.1039/x0xx00000x

Seoyeon Kim,[a] Byung Hak Jhun,[b] Yunjeong Lee,[a] Gayeon Lee,[a] Sihyun Woo,[b] Jaehan Bae,[a] Sohee Lee,[b] Seoyeon Kim,[b] Youngmin You,*[b] and Eun Jin Cho*[a]

A visible-light-driven [2+2] cycloaddition strategy with indole-fused organophotocatalysts (organoPCs) developed in our laboratory is presented, highlighting a sustainable approach with minimal solvent usage and no sacrificial reagents. Mechanistic investigations, supported by spectroscopic analyses and density functional theory (DFT) calculations, suggest that this transformation proceeds via a ground-state association mechanism rather than the more commonly proposed energy transfer pathway. Specifically, noncovalent interactions between the organoPC and a cinnamate substrate enable the formation of a [PC···substrate] complex, which, upon photoexcitation, engages in an efficient route to the triplet state that drives [2+2] cycloaddition. Structural tuning of the organoPC framework proves critical to catalytic performance, as pentacyclic architectures featuring extended π-conjugation display enhanced π–π interactions and the superior reactivity. This design principle facilitates regioselective cycloadditions across a broad range of functionalized cinnamate derivatives, highlighting the versatility and atom economy achievable under visible-light irradiation.

Introduction

Visible-light-driven transformations have garnered considerable interest as environmentally benign and sustainable methodologies in synthetic chemistry.[1] Although metal-based photocatalysts such as Ir and Ru complexes were initially prevalent, concerns regarding their cost, toxicity, and environmental impacts have led to the emergence of organophotocatalysts (organoPCs).[2] These metal-free photocatalysts enable efficient reactions under visible light and are generally more economical and less hazardous than their metallic counterparts.

Photocatalytic reactions commonly follow electron transfer (ET)[3] or energy transfer (EnT)[4] pathways (Figure 1A). EnT is increasingly attractive as it eliminates the need for sacrificial agents typically required in ET processes, enabling direct energy transfer from the photocatalyst to the substrate.[4a-c] The EnT-based photocatalysis often involves triplet–triplet energy transfer for activation of organic substrates.[4] However, unlike Ir- or Ru- based late-transition-metal complexes, organoPCs without heavy elements often suffer from limited triplet activation due to the intrinsically slow intersystem crossing (ISC).[4g] Consequently, alternative approaches are also emerging such as catalytic electron donor–acceptor (EDA) complexes.[5-8] By forming non-covalent, transient assemblies between a photocatalyst and a substrate, EDA complexes can mediate photoactivation without requiring specific redox or energy-transfer criteria—enhancing both reaction scope and sustainability.

Figure 1 Ground State Association-Mediated Photoactivation of Indole-fused OrganoPC

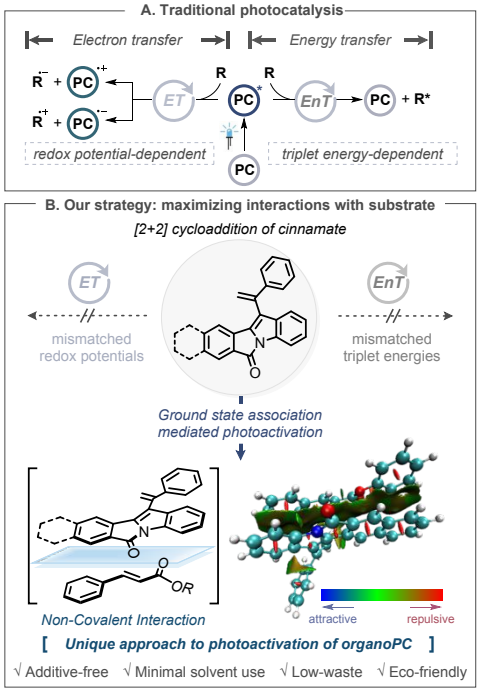

Photochemical [2+2] cycloaddition is a versatile reaction that harnesses photon energy to form cyclobutane frameworks,[9] playing a crucial role in applications ranging from medicinal chemistry to materials science. Herein, we describe a visible-

[a] Department of Chemistry, Chung-Ang University, 84 Heukseok-ro, Dongjak-gu, Seoul 06974, Republic of Korea. E-mail: ejcho@cau.ac.kr (E. J. C.)
[b] Department of Chemical and Biomolecular Engineering, Yonsei University, 50 Yonsei-ro, Seodaemun-gu, Seoul 03722, Republic of Korea. E-mail: odds2@yonsei.ac.kr (Y. Y.)
Supplementary Information available: See DOI: 10.1039/x0xx00000x

View Article Online DOI: 10.1039/D5QO00774G

light-driven [2+2] cycloaddition[9] of cinnamate derivatives,[10] facilitated by our indole-fused organoPC,[11] that forms a transient complex through specific substrate interactions (Figure 1B). Notably, previous examples of cinnamate-based [2+2] cycloadditions have relied exclusively on metal-based photocatalysts.[10b-f,10h] The intrinsic affinity between the indole-fused catalyst and the substrate facilitates photoactivation without the need for strict energetic or electrochemical potential matching. This approach not only broadens the scope of organoPCs in [2+2] cycloaddition reactions but also establishes a highly sustainable strategy. By harnessing interaction-driven photoactivation pathways, the reaction operates efficiently under additive-free conditions, in neat systems or with minimal solvent use.

Results and discussion

Our investigation commenced with the systematic screening of various indole-fused organoPCs[11] for the [2+2] cycloaddition reaction of ethyl cinnamate (**1a**) in tetrahydrofuran (THF) under visible light irradiation using 450 nm 18 W blue light-emitting diodes (LEDs) to afford the corresponding cyclobutane product (**2a**) (Scheme 1). The screening revealed that structural modifications in the organoPCs had a pronounced impact on the catalytic efficiency. Among the tested PCs with the arylalkenyl substituents (**A**–**F**), the pentacyclic organoPC **A**, 13-(1-phenylvinyl)-6H-benzo[5,6]isoindolo[2,1-a]indol-6-one (PBIO), demonstrated markedly superior activity compared to the other tetracyclic organoPCs (**B**–**F**), emphasizing the importance of the additional aryl expansion in the system (entries 1–6). To further investigate the role of the arylalkenyl moiety, we synthesized and evaluated pentacyclic organoPCs **G** and **H** with the arylalkyl substituent and without the substituent, respectively. Interestingly, **G** exhibited notable catalytic activity, suggesting that the alkene moiety was not a critical determinant of reactivity (entry 7). In contrast, the removal of the arylalkenyl moiety in organoPC **H** resulted in a complete loss of catalytic performance, highlighting the critical influence of specific structural features of the aryl substituent in indole-fused organoPCs on their catalytic activity in visible-light-driven [2+2] cycloaddition reactions (entry 8). Notably, the reaction proceeds efficiently even under solvent-free conditions, further highlighting the environmental friendliness of this transformation (entry 10). A comparison between entries 1 and 9 indicates that dilution beyond a certain point does not lead to significant improvements in yield or diastereoselectivity. Therefore, we conducted the reaction at a 5 M concentration to align with green chemistry principles by minimizing solvent use and reducing chemical waste. Additional solvent and wavelength screening results are presented in Table S1 of the Supplementary Information. Moreover, a control experiment conducted in the absence of the photocatalyst, also detailed in Table S1 (entry 2), showed no product formation under the reaction conditions, indicating that direct photoactivation of **1a** is unlikely. Notably, organoPC **A** demonstrates comparable or superior efficiency to commonly used photocatalysts. Neither eosin Y, a widely used organoPC, nor $Ru(bpy)_3(PF_6)_2$,[10b] the most commonly employed Ru-based PC, promoted the reaction at all (entries 11 and 12). Additionally, Ir-based photocatalysts previously used for this transformation (Ir cat. **I**,[10e] Ir cat. **II**[10d,10f,10h]) showed comparable or lower yields (entries 13 and 14), suggesting that **A** serves as an effective metal-free alternative.

Scheme 1 Optimization of Reaction Conditions[a,b]

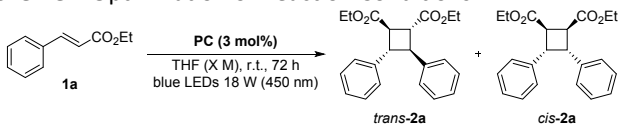

	PC	X	yield (%)	d.r. (*trans*:*cis*)		PC	X	yield (%)	d.r. (*trans*:*cis*)
1	A	5	96	6.4:1	8	H	5	N.R.	-
2	B	5	8	1:1	9	A	1.67	94	6.8:1
3	C	5	0	-	10	A	neat	84	3.9:1
4	D	5	49	4.1:1	11	eosin Y	5	N.R.	-
5	E	5	57	5.1:1	12	Ru cat.	5	N.R.	-
6	F	5	24	4.3:1	13	Ir cat. **I**	5	86	9:1
7	G	5	98	5.7:1	14	Ir cat. **II**	5	93	7.5:1

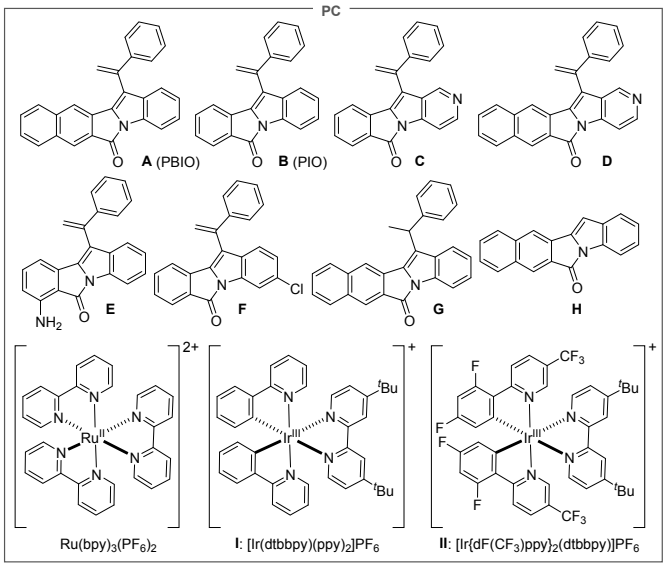

[a]Reaction scale: **1a** (0.1 mmol); [b]Yields were determined by ^{1}H NMR yield using bromoform as an internal standard and diastereomeric ratios (d.r.) were obtained from the ^{1}H NMR spectra of the crude reaction mixtures.

Our investigations shifted to elucidating the photocatalytic reaction mechanism, with a particular focus placed on understanding the distinct reactivity observed between pentacyclic PBIO (**A**) and tetracyclic PIO (**B**) organoPCs, despite their structural similarities. The [2+2] cycloaddition reactions generally proceed via well-established electron[9b,12] or energy[9c,13] transfer mechanisms. To explore the possibility of an electron transfer mechanism, we determined the oxidation (E_{ox}) and reduction (E_{red}) potentials of **A**, **B**, and **1a** using cyclic and differential pulse voltammetry (Scheme 2 and see Supplementary Information, Figure S2 for the voltammograms). We then calculated the excited-state redox potentials of **A** and **B** based on the relationships $E^*_{ox} = E_{ox} - E_{S1}$ and $E^*_{red} = E_{red} + E_{S1}$, where E^*_{ox} is the excited-state oxidation potential, E_{S1} is the S_1 state energy determined from the onset wavelength of the

View Article Online
DOI: 10.1039/D5QO00774C

UV–Vis absorption spectrum (Figure S3 in Supplementary Information), and E^*_{red} is the excited-state reduction potential.[3c,14] These ground- and excited-state redox potentials, compared in Scheme 2a, did not align with either an oxidative or reductive quenching pathway, excluding the electron transfer pathway. Actually, our analyses revealed the endoergic nature of the oxidative quenching of the excited-state **A** (**A***) and **B** (**B***) with the positive free energy changes (ΔG_{ET}) greater than 0.20 and 0.16 eV, respectively. The reductive quenching of **A*** and **B*** by **1a** is also thermodynamically disfavoured with (ΔG_{ET}) values greater than 0.17 and 0.09 eV, respectively.

Scheme 2 Mechanistic Studies

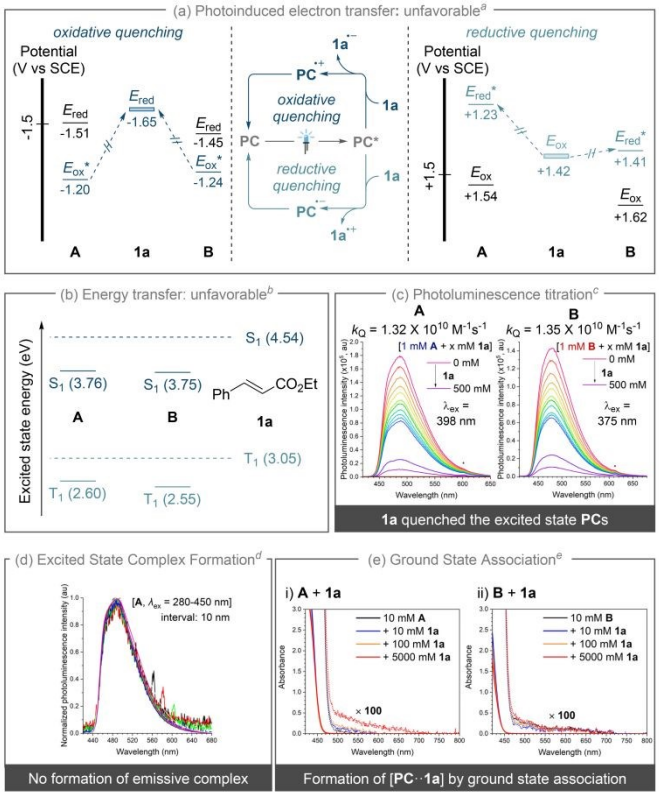

[a]Redox potential diagram: excited-state oxidation potential ($E_{ox}^* = E_{ox} - E_{S1}$), excited-state oxidation potential ($E_{red}^* = E_{red} + E_{S1}$), S_1 state energy determined from the onset wavelength of the UV-Vis absorption spectrum (E_{S1});
[b]Excited state energy diagram: singlet (S_1) and triplet (T_1) state energies of organoPCs **A**, **B** and **1a**, calculated at the ω-B97X-D/TZP//B3LYP-D3(BJ)/TZP level using a solvation method based on the conductor-like screening model parameterized for 1,4-dioxane;
[c]Photoluminescence (fluorescence) spectra of 1.0 mM **A** and **B** containing increasing concentrations of **1a** in deaerated THF;
[d]Normalized photoluminescence spectra of 1.0 mM **A** with added 1000 mM **1a** in THF. (λ_{ex} = 280–450 nm, interval: 10 nm);
[e]UV-Vis absorption of 10 mM (i) **A** and (ii) **B** in THF with increased concentrations of **1a** (10–5000 mM).

Subsequently, we examined the possibility of an energy transfer mechanism—more common in [2+2] photochemical processes. **A** and **B**, and **1a** did not show notable phosphorescence signals even at cryogenic temperatures (~ 78 K). We thus opted to perform quantum chemical calculations based on the ω-B97X-D/TZP//B3LYP-D3(BJ)/TZP level in order to compare the electronic states, including triplet energies, of **A**, **B**, and **1a** (Scheme 2b). Our calculations predicted the T_1 energy levels of **A** (2.60 eV) and **B** (2.55 eV) lower than the T_1 of **1a** (3.05 eV), effectively ruling out a conventional triplet–triplet energy transfer pathway. Furthermore, the S_1 energies of **A** (3.76 eV) and **B** (3.75 eV) are also lower than that of **1a** (4.54 eV). Additionally, no spectral overlap is observed between the emission profiles of **A** or **B** and the absorption spectrum of **1a**, further disfavoring the feasibility of a singlet–singlet energy transfer-based pathway. This energetic disposition, combined with the absence of spectral overlap, directly rebuts the proposed triplet activation mechanism involving singlet–singlet energy transfer from organoPCs to **1a**, followed by ISC of **1a**. This energetic disposition also rebuts the triplet activation mechanism involving singlet–singlet energy transfer from organoPCs to **1a**, followed by ISC of **1a**. Unexpectedly, however, photoluminescence (fluorescence, PL) spectra recorded in Ar-saturated THF solutions of organoPCs (1.0 mM) with increased concentrations of **1a** (0–500 mM) revealed concentration-dependent quenching of the organoPC fluorescence by **1a** (Scheme 2c).

Scheme 3 DFT Calculations and Proposed Mechanism

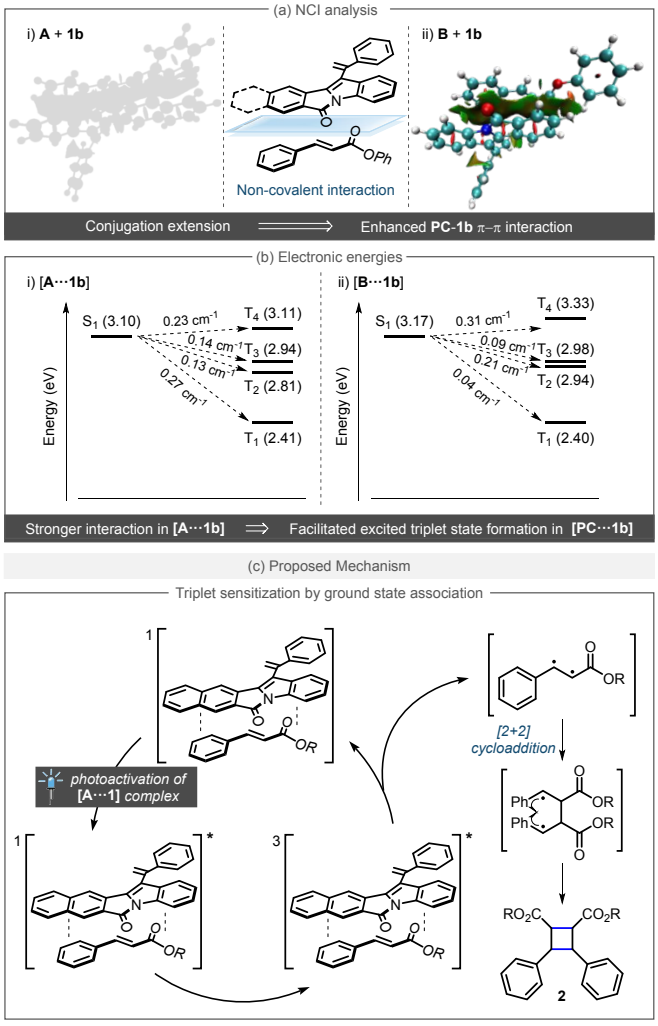

The corresponding rates for bimolecular quenching (k_Qs), which could be calculated through the Stern–Volmer analyses, are as large as 1.32×10^{10} M^{-1} s^{-1} for **A** and 1.35×10^{10} M^{-1} s^{-1} for **B**. Note that these k_Q values are close to the diffusion rate constant in THF at 298 K which can be calculated using the

View Article Online DOI: 10.1039/D5QO00774C

Stokes–Einstein–Sutherland equation (1.44×10^{10} M^{-1} s^{-1}).[15] This similarity suggests that quenching occurs through a pre-associated static catalyst–substrate complex, where nonradiative deactivation of **A*** by **1a** proceeds without requiring diffusion-limited formation of an encounter complex.[4a,4c,16] In addition, the virtually identical k_Q values for the more reactive organoPC **A** and the less reactive organoPC **B** indicate that excited-state processes do not govern the catalysis. Subsequent efforts sought to investigate whether the reaction proceeds via an excited-state complex. PL spectra of 1.0 mM **A** were recorded at varied excitation wavelengths (280–450 nm, in 10 nm increments) in the presence of 1.0 M **1a** (Scheme 2d). Under conditions favoring an emissive excited-state complex, distinct shifts in the PL spectra would be expected. However, no significant spectral variation was observed, effectively ruling out the formation of an emissive excited-state species, such as exciplexes. This absence of PL shift supports that the interaction occurs prior to excitation rather than in the excited state. An alternative hypothesis posited a ground-state association between organoPCs and **1a**. To explore this possibility, UV–Vis absorption spectra were measured for solutions containing 10 mM organoPCs in THF and excess amounts of **1a** (10–5000 mM). As shown in Scheme 2e, in the case of organoPC **A**, a new absorption band emerged in the regions > 500 nm, whose absorbance systematically increased with higher concentrations of **1a**. By contrast, the less reactive organoPC **B** exhibited no discernible change under identical conditions. The association constant between **A** and **1a** was determined to be 0.4 M^{-1} by ^1H NMR titration experiments (see Figure S4 in the Supplementary Information). Despite not conclusive, these observations support a mechanism involving the ground-state complex formation between organoPC **A** and **1a**, thereby providing a rationale for the contrasting reactivities exhibited by **A** and **B**. Although the chemical nature for the ground-state complex needs further spectroscopic resolutions, an EDA complex is unlikely because the UV–vis absorption spectra do not show apparent chromic shifts upon changing organoPCs. Our quantum chemical calculations suggest the association mainly involve a π–π interaction, rather than a charge-transfer interaction.

Subsequent investigations addressed how structural differences between **A** and **B** govern their reactivities, particularly through the ground-state association. Building on earlier observations, the central hypothesis proposed that variations in noncovalent interactions, especially π–π interactions—arising from the additional aryl expansion—underlie the observed differences in catalytic performance. To explore this assumption, density functional theory (DFT) calculations were performed with phenyl cinnamate (**1b**) (Scheme 3a), a substrate chosen to enhance π–π interactions with the multi-ring frameworks of the organoPCs. Results indicated that the pentacyclic **A**, which possesses extended conjugation relative to **B**, exhibits stronger π–π stacking with **1b**, thus explaining **A**'s superior reactivity. Despite sharing the similar core structure, **D** having fused pyridine in place of benzene in **A** yielded a lower reaction yield than **A** (see Scheme 1). The difference likely arose from the decreased polarizability of π electrons in pyridine, which influenced the ability of **D** to form productive associations with the substrate and, consequently, the catalytic performance.[17] Although full understanding of the differed catalytic efficiencies requires further investigations, the results demonstrate strong structure–reactivity dependence of the catalysts. Variations in conjugation length (**A** vs **B**), heteroatom incorporation (**A** vs **D**), and electron-donating or -withdrawing substituents (**B** vs **E** and **F**) result in markedly different reaction yields and diastereoselectivities.

Scheme 4 Substrate Scope[a,b]

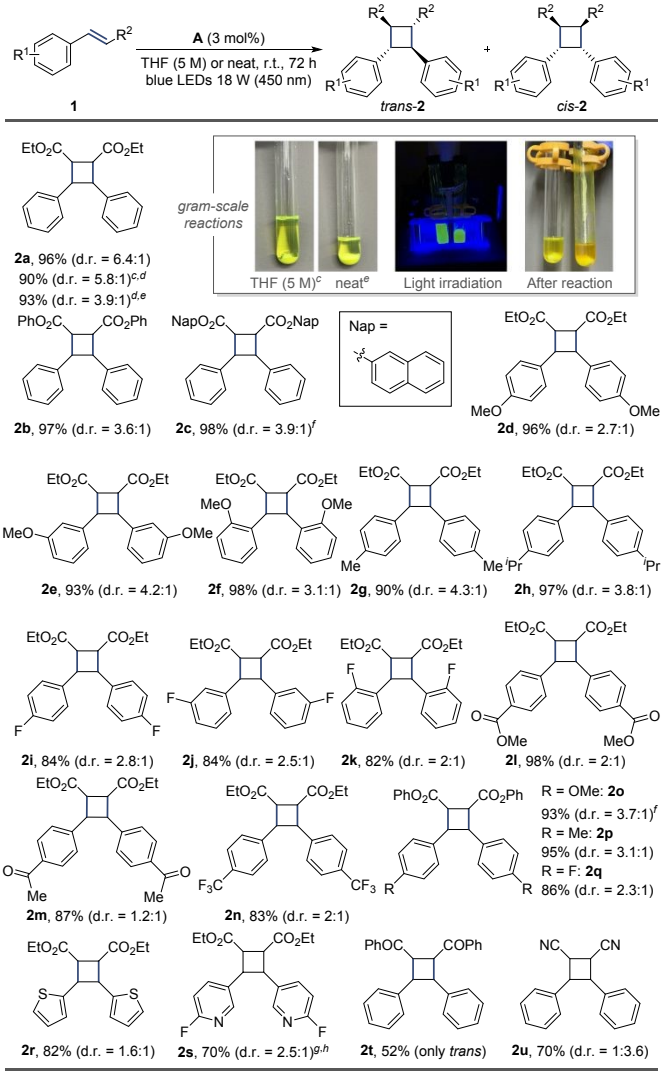

[a]Reaction scale: **1** (0.1 mmol), **A** (3 mol%), THF (20 μL); [b]Yields were determined by ^1H NMR yield using bromoform as an internal standard and diastereomeric ratios were reported in the form of *trans*-**2**:*cis*-**2**; [c]Reaction scale: **1a** (6 mmol), **A** (5 mol%), THF (1.2 mL), 17 days; [d]Conversion based yield was reported; [e]Reaction scale: **1a** (6 mmol), **A** (5 mol%), 17 days; [f]Reaction conditions: THF (1.67 M); [g]Reaction conditions: THF (2.5 M); [h]Conversion-based yield.

Our relativistic DFT calculations further revealed that the [**A**···**1b**] complex would exhibit the stronger ISC between the S_1 and T_1 states (spin–orbit coupling matrix element (SOCME) = 0.27 cm^{-1}) than does the [**B**···**1b**] complex (SOCME = 0.04 cm^{-1}), suggesting that robust noncovalent interactions would facilitate more efficient the triplet formation (Scheme 3b). However, the [**D**···**1b**] complex was calculated to exhibit a greater SOCME

View Article Online
DOI: 10.1039/D5QO00774C

value of 7.09 cm^{-1}, than that of the [**A**···**1b**] complex, although **D** produced a low reaction yield (Scheme 1). These results suggest that the overall catalytic efficiency may not be governed by ISC within the ground-state association complex, although ISC remains essential for triplet activation of **1b**. Our nanosecond laser flash photolysis experiments revealed a long-lived stimulated emission signal (τ = 9.72 μs) from the [**A**···**1**] complex, supporting the formation of a triplet excited species (Figure S5). The proposed mechanism begins with ground-state association between **A** and **1**, forming an [**A**···**1**] complex (Scheme 3c). Upon photoexcitation, this complex reaches a singlet excited state, followed by efficient ISC to the triplet state, from which the [2+2] cycloaddition reaction proceeds to generate the cyclobutane **2**.

Next, under the optimized conditions, we examined the substrate scope of the [2+2] cycloaddition using a diverse range of cinnamate derivatives (**1**) (Scheme 4). Notably, this transformation is exceptionally eco-friendly, proceeding with only the catalyst—without additives—and performing well even without solvent. Furthermore, no byproducts were formed in most of the reactions and PBIO (**A**) was easily removed. Consequently, products were isolated by simple filtration through the plug of silica, without any workup process (see the inset of Scheme 4). Both aliphatic and aromatic cinnamates, including naphthyl-substituted derivatives, exhibited excellent reactivity, yielding the corresponding cyclobutane products with the *trans* isomer as the major product. Notably, the reaction proceeded effectively irrespective of the electronic or positional effects (*ortho*-, *meta*-, *para*-) of substituents on the aromatic ring. The mild, additive-free conditions under visible light irradiation proved highly tolerant to various functional groups. Medicinally relevant substituents such as fluoride (**2i–2k** and **2q**), trifluoromethyl (CF_3, **2n**),[18] and a heteroaryl aryl variants including a thiophene (**2r**) and a pyridyl-substituted cinnamate (**2s**) were also compatible with this transformation. Interestingly, (*E*)-chalcone, a ketone-containing variant, successfully underwent the reaction, albeit with a moderate yield. However, it exhibited excellent diastereoselectivity, exclusively forming the *trans* isomer (**2t**). Unexpectedly, cinnamylnitrile (**2u**) were also compatible with this transformation, affording *cis*-isomer as the major product, possibly due to its linear structure. The relatively lower reactivity compared to ester substrates highlights the role of the ester unit in facilitating pivotal ground-state interactions. Notably, a competitive [2+2] cycloaddition between two highly reactive substrates (**1**) led to the formation of a heterodimer, indicating that both partners participate concurrently in the reaction (see Figure S8 in the Supplementary Information).

Conclusions

This study demonstrates that visible-light-driven [2+2] cycloadditions can be achieved under mild, metal-free conditions using structurally optimized indole-fused organoPCs. Mechanistic investigations, supported by spectroscopic and computational data, revealed that the triplet activation relies on a ground-state association between the organoPC and the substrate, rather than traditional electron or energy transfer pathways. Pentacyclic **A**, characterized by extended conjugation, exhibited exceptional reactivity due to enhanced π–π interactions with cinnamate derivatives. This interaction facilitated efficient substrate transformations across a broad range of derivatives, offering a highly sustainable approach with minimal solvent use and no need for sacrificial reagents. These findings highlight the critical role of rational catalyst design in developing sustainable and selective photocatalysis strategies, paving the way for advancements in visible-light-mediated transformations.

Author contributions

The paper was written through the contributions of all authors.

Conflicts of interest

There are no conflicts to declare.

Data availability

The data supporting this article have been included as part of the Supplementary Information.

Acknowledgements

We gratefully acknowledge support from the National Research Foundation of Korea (RS-2025-00559692, RS-2024-00409659, and RS-2023-00208856).

Notes and references

1 For selective reviews on visible-light photocatalysis, see: (a) L. Marzo, S. K. Pagire, O. Reiser and B. König, Visible-Light Photocatalysis: Does It Make a Difference in Organic Synthesis?, *Angew. Chem. Int. Ed.*, 2018, **57**, 10034-10072; (b) C. R. Stephenson, T. P. Yoon and D. W. MacMillan, *Visible light photocatalysis in organic chemistry*, John Wiley & Sons, 2018; (c) S. D. A. Zondag, D. Mazzarella and T. Nöel, Scale-Up of Photochemical Reactions: Transitioning from Lab Scale to Industrial Production, *Annu. Rev. Chem. Biomol. Eng.*, 2023, **14**, 283-300.

2 For selective reviews on organoPCs, see: (a) S. Fukuzumi and K. Ohkubo, Organic synthetic transformations using organic dyes as photoredox catalysts, *Org. Biomol. Chem.*, 2014, **12**, 6059-6071; (b) I. K. Sideri, E. Voutyritsa and C. G. Kokotos, Photoorganocatalysis, small organic molecules and light in the service of organic synthesis: the awakening of a sleeping giant, *Org. Biomol. Chem.*, 2018, **16**, 4596-4614; (c) M. Uygur and O. G. Mancheño, Visible light-mediated organophotocatalyzed C-H bond functionalization reactions, *Org. Biomol. Chem.*, 2019, **17**, 5475-5489; (d) Y. Lee and M. S. Kwon, Emerging Organic Photoredox Catalysts for Organic Transformations, *Eur. J. Org. Chem.*, 2020, **2020**, 6028-6043; (e) A. Vega-Peñaloza, J. Mateos, X. Companyó, M. Escudero-Casao and L. Dell'Amico, A Rational Approach to Organo-Photocatalysis: Novel Designs and Structure-Property Relationships, *Angew. Chem. Int. Ed.*, 2020, **60**, 1082-1097; (f) M. Kim, S. H. Y. Hong, J. Jeong and S. W. Hong, Visible-Light-

Active Coumarin- and Quinolinone-Based Photocatalysts and Their Applications in Chemical Transformations, *Chem. Rec.*, 2023, **23**, e202200267.

3 For selective reviews on electron transfer, see: (a) J. M. R. Narayanam and C. R. J. Stephenson, Visible light photoredox catalysis: applications in organic synthesis, *Chem. Soc. Rev.*, 2011, **40**, 102-113; (b) C. K. Prier, D. A. Rankic and D. W. C. MacMillan, Visible Light Photoredox Catalysis with Transition Metal Complexes: Applications in Organic Synthesis, *Chem. Rev.*, 2013, **113**, 5322-5363; (c) N. A. Romero and D. A. Nicewicz, Organic Photoredox Catalysis, *Chem. Rev.*, 2016, **116**, 10075-10166; (d) N. L. Reed and T. P. Yoon, Oxidase reactions in photoredox catalysis, *Chem. Soc. Rev.*, 2021, **50**, 2954-2967; (e) N. Holmberg-Douglas and D. A. Nicewicz, Photoredox-Catalyzed C-H Functionalization Reactions, *Chem. Rev.*, 2022, **122**, 1925-2016; (f) S. P. Pitre and L. E. Overman, Strategic Use of Visible-Light Photoredox Catalysis in Natural Product Synthesis, *Chem. Rev.*, 2022, **122**, 1717-1751.

4 For selective reviews on energy transfer, see: (a) F. Strieth-Kalthoff, M. J. James, M. Teders, L. Pitzer and F. Glorius, Energy transfer catalysis mediated by visible light: principles, applications, directions, *Chem. Soc. Rev.*, 2018, **47**, 7190-7202; (b) Q. Q. Zhou, Y. Q. Zou, L. Q. Lu and W. J. Xiao, Visible-Light-Induced Organic Photochemical Reactions through Energy-Transfer Pathways, *Angew. Chem. Int. Ed.*, 2019, **58**, 1586-1604; (c) F. Strieth-Kalthoff and F. Glorius, Triplet Energy Transfer Photocatalysis: Unlocking the Next Level, *Chem*, 2020, **6**, 1888-1903; (d) M. Bera, D. Lee and E. J. Cho, Advances in N-centered intermediates by energy transfer photocatalysis, *Trends Chem.*, 2021, **3**, 877-891; (e) J. Großkopf, T. Kratz, T. Rigotti and T. Bach, Enantioselective Photochemical Reactions Enabled by Triplet Energy Transfer, *Chem. Rev.*, 2021, **122**, 1626-1653; (f) D. S. Lee, V. K. Soni and E. J. Cho, N-O Bond Activation by Energy Transfer Photocatalysis, *Acc. Chem. Res.*, 2022, **55**, 2526-2541; (g) S. Dutta, J. E. Erchinger, F. Strieth-Kalthoff, R. Kleinmans and F. Glorius, Energy transfer photocatalysis: exciting modes of reactivity, *Chem. Soc. Rev.*, 2024, **53**, 1068-1089.

5 For selective reviews on reactions through EDA complex formation, see: (a) G. E. M. Crisenza, D. Mazzarella and P. Melchiorre, Synthetic Methods Driven by the Photoactivity of Electron Donor-Acceptor Complexes, *J. Am. Chem. Soc.*, 2020, **142**, 5461-5476; (b) A. K. Wortman and C. R. J. Stephenson, EDA photochemistry: Mechanistic investigations and future opportunities, *Chem*, 2023, **9**, 2390-2415.

6 For selective examples of catalytic EDA complex formation utilizing ED catalyst, see: (a) I. Bosque and T. Bach, 3-Acetoxyquinuclidine as Catalyst in Electron Donor-Acceptor Complex-Mediated Reactions Triggered by Visible Light, *ACS Catal.*, 2019, **9**, 9103-9109; (b) E. J. McClain, T. M. Monos, M. Mori, J. W. Beatty and C. R. J. Stephenson, Design and Implementation of a Catalytic Electron Donor-Acceptor Complex Platform for Radical Trifluoromethylation and Alkylation, *ACS Catal.*, 2020, **10**, 12636-12641; (c) E. Le Saux, M. Zanini and P. Melchiorre, Photochemical Organocatalytic Benzylation of Allylic C–H Bonds, *J. Am. Chem. Soc.*, 2022, **144**, 1113-1118; (d) Q. L. Zhou, C. G. G. Sun, X. Liu, X. F. Li, Z. Y. Shao, K. Tan and Y. A. Shen, Electron donor-acceptor complex-catalyzed photoredox reactions mediated by DIPEA and inorganic carbonates, *Org. Chem. Front.*, 2022, **9**, 5264-5271; (e) Y. H. Deng, Q. N. Li, M. H. Li, L. F. Wang and T. Y. Sun, Rational design of super reductive EDA photocatalyst for challenging reactions: a theoretical and experimental study, *RSC Adv.*, 2024, **14**, 1902-1908; (f) X. L. Huang, D. L. Zhang, Q. Li, Z. B. Xie, Z. G. Le and Z. Q. Zhu, Visible-Light-Induced C-H Cyanoalkylation of Azauracils with Cycloketone Oxime Esters via Catalytic EDA Complex, *Org. Lett.*, 2024, **26**, 3727-3732; (g) Y. Huo, B. Chen, Z. Xu, X. Ren, R. Qi and C. Wang, Visible-light-driven C(sp3)–H alkylation of heterobenzylic amines via electron donor–acceptor complexes, *Org. Chem. Front.*, 2024, **11**, 205-210; (h) J. D. Lasso, D. J. Castillo-Pazos, J. M. Salgado, C. Ruchlin, L. Lefebvre, D. Farajat, D. F. Perepichka and C. J. Li, A General Platform for Visible Light Sulfonylation Reactions Enabled by Catalytic Triarylamine EDA Complexes, *J. Am. Chem. Soc.*, 2024, **146**, 2583-2592; (i) Y. F. Tan, M. T. Pei, K. Yang, T. T. Zhou, A. H. Hu and J. J. Guo, Catalytic Generation of Pyridyl Radicals via Electron Donor-Acceptor Complex Photoexcitation: Synthesis of 2-Pyridylindole-Based Heterobiaryls, *Org. Lett.*, 2024, **26**, 8084-8089; (j) J. X. Wang, M. C. Fu, L. Y. Yan, X. Lu and Y. Fu, Photoinduced Triphenylphosphine and Iodide Salt Promoted Reductive Decarboxylative Coupling, *Adv. Sci.*, 2024, **11**, 2307241; (k) K. Yoshizawa, B. X. Li, T. Matsuyama, C. Wang and M. Uchiyama, Visible-Light-Driven Germyl Radical Generation via EDA-Catalyzed ET-HAT Process, *Chem. Eur. J.* 2024, **30**, e202401546.

7 For selective examples of catalytic EDA complex formation utilizing EA catalyst, see: (a) T. Morack, C. Mück-Lichtenfeld and R. Gilmour, Bioinspired Radical Stetter Reaction: Radical Umpolung Enabled by Ion-Pair Photocatalysis, *Angew. Chem. Int. Ed.*, 2019, **58**, 1208-1212; (b) D. Lee, V. K. Soni, S. Heo, H. S. Hwang, Y. You and E. J. Cho, Sustainable photoredox chemistry of a transient ternary complex: an unconventional approach toward trifluoromethylated hydroquinones, *Green Chem.*, 2022, **24**, 6481-6486; (c) A. Runemark and H. Sundén, Aerobic Oxidative EDA Catalysis: Synthesis of Tetrahydroquinolines Using an Organocatalytic EDA Active Acceptor, *J. Org. Chem.*, 2022, **87**, 1457-1469; (d) W. Zhou, S. Wu and P. Melchiorre, Tetrachlorophthalimides as Organocatalytic Acceptors for Electron Donor-Acceptor Complex Photoactivation, *J. Am. Chem. Soc.*, 2022, **144**, 8914-8919; (e) J. L. Wei, J. H. Meng, C. F. Zhang, Y. M. Liu and N. Jiao, Dioxygen compatible electron donor-acceptor catalytic system and its enabled aerobic oxygenation, *Nat. Commun.*, 2024, **15**, 1886; (f) T. Xue, C. Ma, L. Liu, C. H. Xiao, S. F. Ni and R. Zeng, Characterization of A π-π stacking cocrystal of 4-nitrophthalonitrile directed toward application in photocatalysis, *Nat. Commun.*, 2024, **15**, 1455.

8 For selective examples utilizing a photocatalyst as the EDA catalyst, see: (a) V. Quint, F. Morlet-Savary, J. F. Lohier, J. Lalevée, A. C. Gaumont and S. Lakhdar, Metal-Free, Visible Light-Photocatalyzed Synthesis of Benzo[*b*]phosphole Oxides: Synthetic and Mechanistic Investigations, *J. Am. Chem. Soc.*, 2016, **138**, 7436-7441; (b) S. Cuadros, G. Goti, G. Barison, A. Raulli, T. Bortolato, G. Pelosi, P. Costa and L. Dell'Amico, A General Organophotoredox Strategy to Difluoroalkyl Bicycloalkane (CF2-BCA) Hybrid Bioisosteres, *Angew. Chem. Int. Ed.*, 2023, **62**, e202303585; (c) P. P. Sen, N. Saha and S. R. Roy, Investigating the Potency of a Phenalenyl-Based Photocatalyst under the Photoelectrochemical Condition for Intramolecular C-S Bond Formation, *ACS Catal.*, 2024, **14**, 907-920; (d) H. Zhao, Y. X. Zong, Y. Sun, G. H. An and J. K. Wang, An Organocatalytic System for *Z*-Alkene Synthesis via a Hydrogen-Bonding-Assisted Photoinduced Electron Donor-Acceptor Complex, *Org. Lett.*, 2024, **26**, 1739-1744.

9 For selective reviews on photocatalytic [2+2] cycloaddition reactions, see: (a) D. Sarkar, N. Bera and S. Ghosh, [2+2] Photochemical Cycloaddition in Organic Synthesis, *Eur. J. Org. Chem.*, 2020, **2020**, 1310-1326; (b) T. Zhang, Y. Zhang and S. Das, Deal;Photoredox Catalysis for the Cycloaddition Reactions, *Chemcatchem*, 2020, **12**, 6173-6185; (c) M. Sicignano, R. I. Rodríguez and J. Alemán, Recent Visible Light and Metal Free Strategies in [2+2] and [4+2] Photocycloadditions, *Eur. J. Org. Chem.*, 2021, **2021**, 3303-3321.

10 For examples on visible light-induced photocatalytic [2+2] cycloadditions of cinnamate derivatives, see: (a) R. Telmesani, S. H. Park, T. Lynch-Colameta and A. B. Beeler, [2+2] Photocycloaddition of Cinnamates in Flow and Development of a Thiourea Catalyst, *Angew. Chem. Int. Ed.*, 2015, **54**, 11521-11525; (b) T. R. Blum, Z. D. Miller, D. M. Bates, I. A. Guzei and T. P. Yoon, Enantioselective photochemistry through Lewis acid-catalyzed triplet energy transfer, *Science*, 2016, **354**, 1391-1395; (c) T. Lei, C. Zhou, M. Y. Huang, L. M. Zhao, B. Yang, C. Ye, H. Y. Xiao, Q. Y. Meng, V. Ramamurthy, C. H. Tung and L. Z. Wu, General and Efficient Intermolecular [2+2] Photodimerization of Chalcones and Cinnamic Acid Derivatives in Solution through Visible-Light Catalysis, *Angew. Chem. Int. Ed.*, 2017, **56**, 15407-15410; (d) S. K. Pagire, A. Hossain, L. Traub, S. Kerres and O. Reiser, Photosensitised regioselective [2+2]-cycloaddition of cinnamates and related alkenes, *Chem. Commun.*, 2017, **53**, 12072-12075; (e) M. E. Daub, H. Jung, B. J. Lee, J. Won, M. H. Baik and T. P. Yoon, Enantioselective [2+2] Cycloadditions of Cinnamate Esters: Generalizing Lewis Acid Catalysis of Triplet Energy Transfer, *J. Am. Chem. Soc.*, 2019, **141**, 9543-9547; (f) A. Abramov, O. Reiser and D. D. Díaz, Effect of Reaction Media on Photosensitized [2+2]-Cycloaddition of Cinnamates, *Chemistryopen*, 2020, **9**, 649-656; (g) Q. A. Wu, F. Chen, C. C. Ren, X. F. Liu, H. Chen, L. X. Xu, X. C. Yu and S. P. Luo, Donor-acceptor fluorophores as efficient energy transfer photocatalysts for [2+2] photodimerization, *Org. Biomol. Chem.*, 2020, **18**, 3707-3716; (h) F. Medici, A. Puglisi, S. Rossi, L. Raimondi and M. Benaglia, Stereoselective [2+2] photodimerization: a viable strategy for the synthesis of enantiopure cyclobutane derivatives, *Org. Biomol. Chem.*, 2023, **21**, 2899-2904.

11 (a) J. Bae, N. Iqbal, H. S. Hwang and E. J. Cho, Sustainable preparation of photoactive indole-fused tetracyclic molecules: a new class of organophotocatalysts, *Green Chem.*, 2022, **24**, 3985-3992; (b) Y. Lee, B. H. Jhun, S. Woo, S. Kim, J. Bae, Y. You and E. J. Cho, Charge-recombinative triplet sensitization of alkenes for DeMayo-type [2+2] cycloaddition, *Chem. Sci.*, 2024, **15**, 12058-12066.

12 For selective examples on [2+2] cycloadditions through electron transfer process, see: (a) M. A. Ischay, M. E. Anzovino, J. Du and T. P. Yoon, Efficient visible light photocatalysis of [2+2] enone cycloadditions, *J. Am. Chem. Soc.*, 2008, **130**, 12886-12887; (b) E. L. Tyson, E. P. Farney and T. P. Yoon, Photocatalytic [2 + 2] cycloadditions of enones with cleavable redox auxiliaries, *Org. Lett.*, 2012, **14**, 1110-1113; (c) A. A. Lee and J. R. Swierk, Mechanistic Investigation of a Photoredox Cycloaddition Chain Reaction, *J. Am. Chem. Soc.*, 2024, **146**, 34900-34908.

13 (a) M. Zhu, X. Zhang, C. Zheng and S. L. You, Energy-Transfer-Enabled Dearomative Cycloaddition Reactions of Indoles/Pyrroles via Excited-State Aromatics, *Acc. Chem. Res.*, 2022, **55**, 2510-2525; (b) P. Franceschi, S. Cuadros, G. Goti and L. Dell'Amico, Mechanisms and Synthetic Strategies in Visible Light-Driven [2+2]-Heterocycloadditions, *Angew. Chem. Int. Ed.*, 2023, **62**, e202217210; (c) A. Palai, P. Rai and B. Maji, Rejuvenation of dearomative cycloaddition reactions via visible light energy transfer catalysis, *Chem. Sci.*, 2023, **14**, 12004-12025; (d) E. Oueis, M. Elkadi and R. Rios, Visible-Light-Driven Cyclizations, *Adv. Synth. Catal.*, 2024, **366**, 635-697; (e) D. Saha, Catalytic Dearomative Cycloaddition Reactions Enabled by Visible Light, *Asian J. Org. Chem.*, 2024, **13**, e202400374.

14 D. Rehm and A. Weller, Kinetics of Fluorescence Quenching by Electron and H-Atom Transfer, *Isr. J. Chem.*, 1970, **8**, 259-271.

15 W. Sutherland, LXXV. A dynamical theory of diffusion for non-electrolytes and the molecular mass of albumin, *The London, Edinburgh, and Dublin Philosophical Magazine and Journal of Science*, 1905, **9**, 781-785.

16 (a) S. De Kreijger, F. Glaser and L. Troian-Gautier, From photons to reactions: key concepts in photoredox catalysis, *Chem Catal.*, 2024, **4**, 101110; (b) C. Wang, H. Li, T. H. Burgin and O. S. Wenger, Cage escape governs photoredox reaction rates and quantum yields, *Nat. Chem.*, 2024, **16**, 1151-1159.

17 (a) E. G. Hohenstein and C. D. Sherrill, Effects of heteroatoms on aromatic pi-pi interactions: benzene-pyridine and pyridine dimer, *J. Phys. Chem. A*, 2009, **113**, 878-886; (b) J. I. Seo, I. Kim and Y. S. Lee, π-π Interaction energies in monosubstituted-benzene dimers in parallel- and antiparallel-displaced conformations, *Chem. Phys. Lett.*, 2009, **474**, 101-106; (c) C. Sutton, M. S. Marshall, C. D. Sherrill, C. Risko and J. L. Brédas, Rubrene: The Interplay between Intramolecular and Intermolecular Interactions Determines the Planarization of Its Tetracene Core in the Solid State, *J. Am. Chem. Soc.*, 2015, **137**, 8775-8782; (d) N. J. Silva, F. B. C. Machado, H. Lischka and A. J. A. Aquino, π-π stacking between polyaromatic hydrocarbon sheets beyond dispersion interactions, *Phys. Chem. Chem. Phys.*, 2016, **18**, 22300-22310; (e) S. K. Park, J. H. Kim and S. Y. Park, Organic 2D Optoelectronic Crystals: Charge Transport, Emerging Functions, and Their Design Perspective, *Adv. Mater.*, 2018, **30**, 1704759; (f) L. Q. Jing, P. D. Li, Z. Li, D. L. Ma and J. G. Hu, Influence of π-π interactions on organic photocatalytic materials and their performance, *Chem. Soc. Rev.*, 2025, **54**, 2054-2090.

18 (a) T. Chatterjee, N. Iqbal, Y. You and E. J. Cho, Controlled Fluoroalkylation Reactions by Visible-Light Photoredox Catalysis, *Acc. Chem. Res.*, 2016, **49**, 2284-2294; (b) E. J. Cho, Radical-Mediated Fluoroalkylations, *Chem. Rec.*, 2016, **16**, 47-63; (c) C. H. Ka, S. Kim and E. J. Cho, Visible Light-Induced Metal-Free Fluoroalkylations, *Chem. Rec.*, 2023, **23**, e202300036.

View Article Online
DOI: 10.1039/D5QO00774G

Data availability

The data underlying this study are available in the published article and its Supplementary Information.